NASA TECHNICAL NOTE

NASA TN D-4035

LAMINAR FLOW ANALYSIS OF FILM BOILING FROM A HORIZONTAL WIRE

by Kenneth J. Baumeister and Thomas D. Hamill

Lewis Research Center
Cleveland, Ohio

NATIONAL AERONAUTICS AND SPACE ADMINISTRATION • WASHINGTON, D. C. • JULY 1967

LAMINAR FLOW ANALYSIS OF FILM BOILING FROM A HORIZONTAL WIRE

By Kenneth J. Baumeister and Thomas D. Hamill

Lewis Research Center
Cleveland, Ohio

NATIONAL AERONAUTICS AND SPACE ADMINISTRATION

For sale by the Clearinghouse for Federal Scientific and Technical Information
Springfield, Virginia 22151 – CFSTI price $3.00

CONTENTS

LAMINAR FLOW ANALYSIS OF FILM BOILING FROM A HORIZONTAL WIRE

by Kenneth J. Baumeister and Thomas D. Hamill

Lewis Research Center

SUMMARY

The heat-transfer coefficient for pool film boiling from a horizontal wire was analyzed by subdividing the wire into many cells and analyzing the behavior of a particular cell. A cell consists of a vapor dome and the thin annular film around it, and is assumed to be a time-averaged configuration of the actual situation in which vapor domes are growing and vapor is escaping.

If it is assumed that the steady-state equations can be applied to the time-averaged configuration, the Navier-Stokes equations with inertia terms neglected, the continuity equation, and the energy equation with convective terms neglected can be solved simultaneously to obtain the heat-transfer coefficient for horizontal wires in film boiling. Also, the cell size was assumed to adjust itself to maximize the rate of heat transport.

The heat-transfer coefficient h_w is given by

$$h_w = 0.373\left[\frac{k^3 H^* a(\rho_l - \rho_v)\rho_v}{\mu(T_w - T_{sat})l}\right]^{1/4}\left[1 + \frac{9}{\sqrt{6}}\frac{l}{D_o} + \frac{8}{3\sqrt{6}}\left(\frac{l}{D_o}\right)^3\right]^{1/4}$$

where l is a characteristic length $\left[g_c\sigma/a(\rho_l - \rho_v)\right]^{1/2}$, a the acceleration of gravity, k the vapor thermal conductivity, H^* an effective heat of vaporization, ρ_l and ρ_v the liquid and vapor densities, respectively, μ the absolute vapor viscosity, T_w and T_{sat} the wire and surface temperatures, respectively, D_o the wire diameter, and g_c a conversion factor in Newton's law of motion (carried only as a convenience for workers in British units - not necessary in cgs system). This expression agrees with the experimental data tabulated by Breen and Westwater for wires with l/D_o ratios of 0.015 to 50.0.

INTRODUCTION

Film-boiling heat transfer is important to such diverse fields as cryogenics where even a relatively low wall temperature will induce film boiling, or in quenching where the high initial temperature of the metal produces film boiling. Film boiling can occur for discrete amounts of liquid such as in Leidenfrost film boiling or on submerged heating surfaces. In film boiling, a layer of hot vapor supports a layer of dense fluid. Thus, in a gravitational field this situation is inherently unstable. For example, figure 1(a), displaying a photograph from reference 1, shows the form that the instabilities take. At regularly spaced intervals along the wire, the vapor will break through and escape under the influence of gravity into the bulk liquid (see ref. 2 for additonal photographs).

Film boiling, as shown in figure 1, is characterized by a thin annular vapor blanket covering the wire, by spatially periodic domes in which the distance between domes is nearly constant with time, and by a temporal periodicity - the birth, growth, and departure of a vapor dome which represent some average cycle time. This investigation was conducted to determine the heat-transfer and geometric characteristics of this phenomenon.

In one of the earliest works on film boiling, Bromley (ref. 3) presented an analytical model for film boiling around large tubes. Later, Breen and Westwater (ref. 4) extended Bromley's correlation to film boiling from small wires, and concluded that the critical wavelength λ_c of hydrodynamic stability theory

$$\lambda_c = 2\pi\left[\frac{g_c\sigma}{a(\rho_l - \rho_v)}\right]^{1/2} \tag{1}$$

was an important parameter. (All symbols are defined in appendix A.) They correlated a large amount of experimental data by a semiempirical modification of Bromley's equation:

$$h = \left[\frac{k^3\rho_v(\rho_l - \rho_v)H^*a}{\mu(T_w - T_{sat})\lambda_c}\right]^{1/4}\left(0.59 + 0.069\frac{\lambda_c}{D_o}\right) \tag{2}$$

where the modified latent heat H^*, which takes into account sensible heating in the vapor film, is given by

$$H^* = H_{fg}\left[1 + \frac{0.34\, C_v(T_w - T_{sat})}{H_{fg}}\right]^2 \tag{3}$$

In particular, for tube diameters much greater than the critical wavelength, equation (2) reduces to

$$h_\infty = 0.59\left[\frac{k^3\rho_v(\rho_l - \rho_v)H^*a}{\mu(T_w - T_{sat})\lambda_c}\right]^{1/4} \tag{4}$$

which, except for a constant, is identical in form to Berenson's equation (ref. 5) for a flat plate.

In this report, the laminar film-boiling model is employed. The predicted heat-transfer coefficients agree with the tabulated experimental data of Breen and Westwater for wire diameters as small as 0.00053 centimeter and as large as 4.6 centimeters.

In addition, in the limiting condition of small wires, the predicted heat-transfer coefficient h_w is proportional to (λ_c/D_o) to the 0.75 power rather than to the first power as used by Breen and Westwater. This agrees with the experimental data and implies that, for very small wires, surface tension dominates the gravitational effects.

The authors would like to thank Professor Westwater for the use of his original data plots which had previously been published in reference 4.

BASIC MODEL AND EQUATIONS

Figure 1(a) provides justification for the idealized geometric model of film boiling shown in figures 1(b) and 2. This model consists of a thin tubular vapor film between the wire and the liquid, with vapor escape points indicated by the dome-shaped areas. This cellular pattern is distributed in a periodic fashion along the wire with a wavelength equal to λ.

The major portion of the heat transport is assumed to occur across the thin vapor

film of the tubular portion of the cell. The domes are considered to be so thick that essentially no heat is conducted through them. Physically, the domes act as hydrodynamic sinks into which the vapor generated in the annular region is released. A cell consists of a vapor dome and an annulus in which heat transfer to the liquid takes place by conduction, convection, and radiation through a superheated vapor film; however, in this analysis, radiation and convection are neglected. The assumption is made that the heat transferred from the wire evaporates the liquid from the interface and that the vapor flows in a laminar manner, as indicated by the arrows in figure 2, into the dome-shaped sink.

The vapor dome grows as the vapor enters, breaks away from the wire, and escapes into the bulk liquid (see fig. 1(a)). This growth and escape cycle of the vapor dome repeats itself. The proposed model assumes the existence of a time-averaged configuration where all the velocity, pressure, and temperature fields are at steady state. Thus, this statistically idealized configuration (fig. 2) represents an average "snapshot" of the actual system.

The following additional assumptions are made in developing the analytical model:

(1) The inertia terms in the Navier-Stokes equation are negligible compared to the viscous terms. This assumption can be justified on the ground that the small thickness of the film prevents the buildup of sizeable velocities. Additional support is given to this assumption by references 6 and 7, which consider the Leidenfrost film boiling of drops.

(2) In the tubular portion, a uniform vapor gap thickness between the wire and the liquid is assumed. Photographic evidence (see fig. 1(a)) justifies this assumption.

(3) The axial conduction term in the energy equation is assumed to be negligible in comparison with the radial term,

$$\frac{\partial^2 T}{\partial x^2} << \frac{1}{r}\frac{\partial}{\partial r}\left(r\frac{\partial T}{\partial r}\right) \tag{5}$$

(4) Sensible heating is accounted for in the final correlation of the heat-transfer coefficient by replacing the latent heat term H_{fg} with the modified latent heat H^* that was presented by Breen and Westwater (eq. (3)).

(5) The liquid-vapor interface is at the saturation temperature, and evaporation takes place uniformly.

(6) The velocity and temperature profiles at any instant are assumed to be in steady state, and the properties of the flow field are evaluated at the film temperature given by

$$T_f = \frac{T_w + T_{sat}}{2} \tag{6}$$

(7) The bulk liquid temperature is taken to be at the saturation temperature and radiation from the wire to the liquid is assumed to be negligible.

The governing equations in cylindrical coordinates subject to the preceding assumptions are as follows:

Momentum:

$$-\frac{g_c}{\rho_v}\frac{\partial P}{\partial r}+\nu\left(\frac{\partial^2 u}{\partial r^2}+\frac{1}{r}\frac{\partial u}{\partial r}-\frac{u}{r^2}+\frac{\partial^2 u}{\partial x^2}\right)=0 \tag{7}$$

$$-\frac{g_c}{\rho_v}\frac{\partial P}{\partial x}+\nu\left(\frac{\partial^2 w}{\partial r^2}+\frac{1}{r}\frac{\partial w}{\partial r}+\frac{\partial^2 w}{\partial x^2}\right)=0 \tag{8}$$

Continuity:

$$\frac{\partial u}{\partial r}+\frac{u}{r}+\frac{\partial w}{\partial x}=0 \tag{9}$$

Energy:

$$\frac{\partial}{\partial r}\left(r\frac{\partial T}{\partial r}\right)=0 \tag{10}$$

The boundary conditions for the differential equations are the following:

At the surface of the wire (fig. 2):

$$\left.\begin{array}{c} r = R_0 \\ u(R_0, x) = w(R_0, x) = 0 \\ T(R_0, x) = T_w \end{array}\right\} \tag{11}$$

At the liquid interface:

$$\left.\begin{aligned} r &= R_1 \\ u(R_1, x) &= u(R_1) \\ w(R_1, x) &= 0 \\ T(R_1, x) &= T_{sat} \end{aligned}\right\} \tag{12}$$

From axial symmetry:

$$\left.\begin{aligned} x &= 0 \\ w &= 0 \quad \text{from} \quad R_0 \leq r \leq R_1 \end{aligned}\right\} \tag{13}$$

In addition, since the values of R_1 and $u(R_1)$ in the boundary conditions of equation (12) are unknowns, an interface energy balance and a pressure balance are also required to make the problem determinate. The interface energy balance is given by

$$-\rho_v H_{fg} u(R_1) = q = -k \left.\frac{\partial T}{\partial r}\right|_{r=R_1} \tag{14}$$

and the pressure balance by

$$\int_0^{x_a} P(R_1, x) 2\pi R_1 \, dx = 2\pi R_1 x_a \bar{P}_s \tag{15}$$

where $\bar{P}_s$ is assumed to be the average pressure in the vapor at the liquid-vapor interface resulting from the weight of the supported liquid, atmospheric pressure, and surface tension effects (see appendix C). Equation (14) expresses an interface energy balance which assumes that all the heat conducted through the vapor vaporizes the liquid.

In addition, since the two geometric parameters λ and x_a are unknowns two additional assumptions are needed.

The first assumption

$$\lim_{R_0 \to \infty} \frac{h_w}{h_\infty} = 1 \tag{16}$$

expresses in mathematical form the experimental observation of Breen and Westwater, as discussed in the introduction, that the heat-transfer coefficient for large wires can be calculated by equation (4). As is shown herein, this assumption is, in effect, equivalent to using experimental data to determine an unknown constant in the analysis. The second assumption

$$\left.\begin{aligned} \frac{\partial h_w}{\partial \lambda} &= 0 \\ \frac{\partial^2 h_w}{\partial \lambda^2} &< 0 \end{aligned}\right\} \tag{17}$$

represents a hypothesis put forward by the authors in reference 8 that the cell wavelength λ adjusts itself to maximize the heat removal rate from the surface. In film boiling, the liquid-vapor interface is a free boundary that can be deformed in such a way as to optimize (in this case, maximize) the heat removal rate from the wire.

From a mathematical point of view, the problem is now completely formulated. For each dependent variable (unknown), there is an appropriate equation or constraint. From this point on, the solution of the equations is merely a matter of integration and some algebraic simplifications. The details of the analytical procedure are given in appendixes B to F. However, the general method and principal results of the analysis are discussed briefly in the next section.

DISCUSSION OF ANALYSIS

The flow equations, momentum and continuity, were converted into a single fourth-order partial differential equation (eq. (B3)) by the introduction of the stream function and this equation was then solved by separation of variables. A velocity distribution was found in terms of one unknown constant of integration β^2 and a dimensionless parameter Δ, where

$$\Delta = \frac{R_1}{R_0} \tag{18}$$

The constant of integration β^2 was evaluated by a static pressure balance giving an evaporation velocity of the form

$$u(\Delta) = \frac{1}{R_0} \left\{ \frac{(1 - \xi_a)\frac{\lambda}{2}\frac{a}{g_c}(\rho_l - \rho_v) - \frac{2\sigma}{(1 - \xi_a)\frac{\lambda}{2}} + \frac{\sigma}{\Delta R_0}}{\frac{16\mu}{3g_c R_0^2}\left(\frac{\lambda}{2R_0}\right)^2 \xi_a^2} \right\} \times \left[\frac{(\ln \Delta)(1 - \Delta^4) + (\Delta^2 - 1)^2}{\Delta \ln \Delta} \right] \tag{B47}$$

The energy transport in the vapor film must now be considered. In terms of the dimensionless coordinate η given by

$$\eta = \frac{r}{R_0} \tag{19}$$

The energy equation (eq. (10)) becomes

$$\frac{\partial}{\partial \eta}\left(\eta \frac{\partial T}{\partial \eta}\right) = 0 \tag{20}$$

Equation (20) has the solution for the temperature

$$T = T_w - \frac{(T_w - T_{sat})\ln \eta}{\ln \Delta} \tag{21}$$

and for the temperature gradient

$$\frac{\partial T}{\partial \eta} = - \frac{T_w - T_{sat}}{\eta \ln \Delta} \tag{22}$$

Combining the expression for the temperature gradient with the expression for $u(\Delta)$ in the energy balance at the liquid-vapor interface (see appendix D) gives

$$(\Delta^2 - 1)^2 + (1 - \Delta^4)\ln \Delta = - \frac{\dfrac{16\, k(T_w - T_{sat})\mu\left(\dfrac{\lambda}{2R_0}\right)^2 \xi_a^2}{3\rho_v H_{fg} g_c R_0^2}}{(1 - \xi_a)\dfrac{\lambda}{2}\dfrac{a}{g_c}(\rho_l - \rho_v) - \dfrac{2\sigma}{(1 - \xi_a)\dfrac{\lambda}{2}} + \dfrac{\sigma}{\Delta R_0}} \tag{D4}$$

This equation relates the parameter Δ to the fluid properties and cell geometry. The parameters λ and ξ_a are unknowns, whereas the liquid and vapor properties, as well as the radius of the wire, are, of course, known quantities.

Attention is now directed to obtaining an expression for the heat-transfer coefficient from the wire in terms of the quantity Δ. In appendix E, the heat-transfer coefficient (eq. (E8) is shown to be

$$h_w = \frac{k\Psi(R_0, \xi_a)}{R_0 \ln \Delta} \tag{E8}$$

where h_w is the overall heat-transfer coefficient from the wire and $\Psi(R_0, \xi_a)$ represents the fraction of the total area in which the heat is being conducted into the liquid. The first term in equation (E8) expresses the heat-transfer coefficient for a purely conducting hollow cylinder. The fraction term $\Psi(R_0, \xi_a)$ is added to indicate that the vapor dome decreases the effective heat-transfer area.

Maximizing the heat-transfer coefficient with respect to λ according to equation (17) (see appendix E) now yields a value for the cell wevelength λ of the form

$$\frac{\lambda}{2} = \frac{l^2}{(1 - \xi_a)\Delta R_0}\left[\left(1 + \frac{6\Delta^2 R_0^2}{l^2}\right)^{1/2} - 1\right] \tag{E12}$$

where the characteristic length l is defined as

$$l = \left(\frac{g_c \sigma}{a(\rho_l - \rho_v)}\right)^{1/2} \tag{E13}$$

The model proposed for this analysis is strictly applicable to boiling from small wires. As shown in appendix C, the model does not apply for length to diameter ratios less than 0.35. However, the functional form of the analytical result was such that for length to diameter ratios less than 0.35 the data could be conveniently correlated by setting one product of Ψ and ξ_a equal to a experimently determined constant.

HEAT-TRANSFER COEFFICIENT

The following two approximations are convenient to use in determining a heat-transfer coefficient because of the complications arising from the ξ_a factor:

(1) The expression on the left side of equation (D4) is approximated by the expression

$$(\Delta^2 - 1)^2 + (1 - \Delta^4)\ln \Delta = -\frac{4}{3}(\Delta - 1)^4 \tag{23}$$

This expression results from a Taylor Series expansion about $\Delta = 1$ in which terms beyond the fourth power were neglected. As shown in figure 3, this approximation is reasonably accurate over a range of Δ from 1 to 2.4. This range represents those values usually seen in practical experiments.

(2) The expression for the heat-transfer coefficient given by equation (E8) is written in approximate form by letting

$$\ln \Delta \simeq (\Delta - 1) \tag{24}$$

which leads to

$$h_w = \frac{k}{R_0(\Delta - 1)}\Psi(R_0, \xi_a) = \frac{k}{\delta}\Psi(R_0, \xi_a) \tag{25}$$

where δ is the vapor-gap thickness.

When these approximations (eqs. (23) and (24), as well as eq. (16)) are used, the expression for the heat-transfer coefficient simplifies to the following form (see appendix F for details)

$$h_w = 0.373\left[\frac{k^3 H^* a(\rho_l - \rho_v)\rho_v}{\mu(T_w - T_{sat})l}\right]^{1/4} \Gamma^{1/4} \tag{F15}$$

where

$$\Gamma(\Delta, R_0, l) = \frac{3\sqrt{6}}{2l\Lambda}\left(1 - \frac{2}{l^2\Lambda^2} + \frac{1}{\Delta R_0 \Lambda}\right) \tag{26}$$

and

$$\Lambda = \frac{1}{\Delta R_0}\left[\left(1 + \frac{6\Delta^2 R_0^2}{l^2}\right)^{1/2} - 1\right] \tag{27}$$

The latent heat of vaporization H_{fg} was replaced by the modified latent heat of vaporization H^* (eq. (3)) to take into account sensible heating effects.

In general, the unknown value of Δ in the preceding equations is a function of the fluid and system properties and must be evaluated from the governing equations. However, since ξ_a was not evaluated, some approximate value of Δ based on experimental data must be chosen. Convenience dictates that one average value of Δ be chosen over the range of practical interest. The value of Δ becomes significant in the expression for the heat-transfer coefficient only for small wire diameters. For large wires, the terms containing Δ in equation (26) become small relative to 1 and the value of Δ, itself, approaches 1. However, for small wires, this is not the case. For example, the value of Δ estimated from figure 1(a) is near 2. The choice of an average value of Δ to be used in equation (F15) was made by a comparison of theory with the experimental results.

The heat-transfer correlation (eq. (F15)) was plotted with Breen and Westwater's tabulated data in figure 4(a) for various values of Δ. An arbitrary choice of $\Delta = 1$, the lowest physically acceptable value of Δ, best correlates the data. Thus, the equation for the heat-transfer coefficient is

$$h_w = 0.373\left[\frac{k^3 H^* a(\rho_l - \rho_v)\rho_v}{\mu(T_w - T_{sat})l}\right]^{1/4} \Gamma_1^{1/4} \tag{28}$$

where

$$\Gamma(\Delta = 1) = \Gamma_1 = \frac{3\sqrt{6}\, R_0}{2\ell\left[\left(1 + \frac{6R_0^2}{\ell^2}\right)^{1/2} - 1\right]}\left\{1 - \frac{2R_0^2}{\ell^2\left[\left(1 + \frac{6R_0^2}{\ell^2}\right)^{1/2} - 1\right]} + \frac{1}{\left(1 + \frac{6R_0^2}{\ell^2}\right)^{1/2} - 1}\right\} \tag{29}$$

and

$$\Lambda = \frac{1}{R_0}\left[\left(1 + \frac{6R_0^2}{\ell^2}\right)^{1/2} - 1\right] \tag{30}$$

As shown in figure 4(b), the correlation in equation (28) fits the data reasonably well. The correlations of Bromely, and Breen and Westwater are also shown. The data in figure 4 are for 10 liquids (isopropanol, Freon 113, benzene, carbon tetrachloride, ethanol, nitrogen, pentane, oxygen, water, and helium), as listed in reference 4.

SIMPLIFIED EXPRESSION FOR HEAT-TRANSFER COEFFICIENT

The expression for the heat-transfer coefficient (eq. (28)), simplifies when Γ is expressed in terms of its limiting values for small and large wires. For large wires, equation (30) reduces approximately to

$$\Lambda_L \simeq \frac{\sqrt{6}}{\ell} \tag{31}$$

while for small wires

$$\Lambda_S \simeq \frac{3R_0}{\ell^2} \tag{32}$$

where the subscripts L and S indicate large and small, respectively. Substituting these expressions into equation (26) and setting Δ equal to 1, as before, give for large wires

$$\Gamma_L = 1 + \frac{3}{2\sqrt{6}} \frac{l}{R_0} \tag{33}$$

whereas for small wires

$$\Gamma_S = \frac{3}{\sqrt{6}} \frac{l}{R_0} + \frac{1}{3\sqrt{6}} \left(\frac{l}{R_0}\right)^3 \tag{34}$$

Taking the value of Γ as the sum of its asymtotic expressions gives

$$\Gamma_A \cong \Gamma_L + \Gamma_S = 1 + \frac{9}{2\sqrt{6}} \frac{l}{R_0} + \frac{1}{3\sqrt{6}} \left(\frac{l}{R_0}\right)^3 \tag{35}$$

Substituting the asymtotic value of Γ given by equation (35) into the expression for the heat-transfer coefficient, equation (28), yields

$$h_w = 0.373 \left[\frac{k^3 H^* a(\rho_l - \rho_v)\rho_v}{\mu(T_w - T_{sat})l}\right]^{1/4} \left[1 + \frac{9}{\sqrt{6}} \frac{l}{D_o} + \frac{8}{3\sqrt{6}} \left(\frac{l}{D_o}\right)^3\right]^{1/4} \tag{36}$$

Figure 4(c) compares the exact expression for the heat-transfer coefficient, equation (28), with the approximate expression, equation (36). Both equations correlate the data; however, equation (36) is the simpler to use.

EFFECT OF ACCELERATION ON FILM BOILING

Multiplying by g/g each term in equation (36) where the acceleration a appears and rearranging give

$$h_w = 0.373 \left[\frac{k^3 H^* (\rho_l - \rho_v)\rho_v}{\mu(T_w - T_{sat})} \frac{g}{l_g}\right]^{1/4} \left[\left(\frac{a}{g}\right)^{3/2} + \frac{9}{\sqrt{6}} \frac{a}{g} \frac{l_g}{D_o} + \frac{8}{3\sqrt{6}} \left(\frac{l_g}{D_o}\right)^3\right]^{1/4} \tag{37}$$

where

$$\ell_g = \left[\frac{g_c \sigma}{g(\rho_\ell - \rho_v)}\right]^{1/2} \tag{38}$$

and g is a reference acceleration of gravity.

The acceleration effect on the heat-transfer coefficient is closely related to the wire diameter. For small length to diameter ratios (large wires), the heat-transfer coefficient varies nearly as the 0.375 power of a; while for medium length to diameter ratios, where the second term in equation (37) dominates, the heat-transfer coefficient varies as the 1/4 power of a. For the limiting case of very thin wires, where the third term in equation (37) dominates, the heat-transfer coefficient is independent of the acceleration a. Equation (37) indicates that no conclusions about gravitational effects on film boiling are possible unless the wire diameter is also considered.

Care must be taken when considering ratios of a/g greater than 1. For the case of a small wire where the length to diameter ratio is large, the third term in equation (37) dominates, and the heat-transfer coefficient is nearly independent of gravity. However, a sufficient increase in a would increase the effect of the first two terms in equation (37).

Figure 5 shows the heat-transfer coefficient for various values of a/g on a 0.476-centimeter tube in a Freon 113 film-boiling system for the data of Pomerantz (ref. 9). As shown in figure 5, the theory agrees closely with experiment, except at low values of a/g. However, the experimental data could conceivably be slightly high for low values of a/g, since the heat-transfer coefficient appears to converge to a value of 1.1 instead of the expected value of 1. Correlations by Pomerantz (ref. 9), Breen and Westwater (ref. 4), and Bromely (ref. 3) are also shown in figure 5.

LARGE WIRE STABILITY

In appendix C, the analytical model was shown to be limited to wire diameters such that $\ell/D_o > 0.35$. This limit is very interesting in light of the observation by Breen and Westwater (ref. 4) that the heat-transfer coefficients for film boiling are not monotonic functions of the tube diameter. Figure 6 shows a plot of the heat-transfer coefficient as a function of tube diameter, as given in reference 4. A possible explanation for the dip and rise in the heat-transfer coefficient is a transition from annular flow associated with thin-wire film boiling to circumferential flow associated with large-wire film boiling. Thus, in the vicinity of ℓ/D_o equal to 0.35, the heat-transfer coefficient could rise very slightly for increasing wire diameters because of a shift in the flow

pattern, as illustrated in figure 4(c). The circumferential flow is probably turbulent in nature.

CONCLUSIONS

A semitheoretical expression for the heat-transfer coefficient associated with pool film boiling from a horizontal wire was derived with the assumption that the system adjusts itself to maximize the heat transfer. The derived expression agrees with all available experimental data, for wire diameters as small as 0.00053 centimeter and as large as 4.6 centimeters, as shown in figure 4(c). For very small wires, the theoretical expression for the heat-transfer coefficient increases to the 0.75 power of length to diameter ratio. In addition, the heat-transfer coefficient is shown to be a function of gravitational acceleration to the 0.375 power for large wires and to the zero power for very small wires. The gravitational relation of the heat-transfer coefficient agrees with the experimental data of Pomerantz for large diameter wires.

Lewis Research Center,
National Aeronautics and Space Administration,
Cleveland, Ohio, February 24, 1967,
129-01-11-02-22.

APPENDIX A

SYMBOLS

A_{ann}	heating area of annular cell region, cm^2
A_{cell}	total heating area of cell, $2\pi R_0 \lambda$, cm^2
a	acceleration of gravity, cm/sec^2
$a_{1, \ldots, 4}$	arbitrary constants
$C_{1, \ldots, 5}$	arbitrary constants
C_v	vapor specific heat at constant volume, $cal/(g)(^oK)$
D_o	wire diameter, cm
d	distance, cm (see fig. 8)
E^2	differential operator defined by eq. (B4)
$F(\xi)$	arbitrary function
f	arbitrary function (see eq. (B5))
G	arbitrary function (see eq. (B5))
g	reference acceleration of gravity, cm/sec^2
g_c	conversion factor in Newton's law of motion, 1.0 g-cm/(sec^2)(dyne) (or 32.17 (lb mass)(ft)/(lb force)(sec^2) for British system)
H^*	modified latent heat of vaporization defined by eq. (3), cal/g
$H(\eta)$	arbitrary function
H_{fg}	latent heat of vaporization, cal/g
h	heat-transfer coefficient, $cal/(cm^2)(sec)(^oK)$
h_{exp}	experimentally determined heat-transfer coefficient, $cal/(cm^2)(sec)(^oK)$
h_w	heat-transfer coefficient from wire, $cal/(cm^2)(sec)(^oK)$
h_∞	heat-transfer coefficient from large wire defined by eq. (4), $cal/(cm^2)(sec)(^oK)$
k	vapor thermal conductivity, $cal/(cm)(sec)(^oK)$
l	characteristic length given by eq. (E13), cm
l_g	characteristic length evaluated at a = g (see eq. (38)), cm
P	absolute pressure, $dyne/cm^2$
P_B	pressure beneath wire at liquid-vapor interface, $dyne/cm^2$
P_l	liquid pressure at liquid-vapor interface, $dyne/cm^2$
P_o	pressure at apex of vapor dome, $dyne/cm^2$
$\overline{P}_s$	average system pressure in vapor, $dyne/cm^2$
P_1	pressure at base of vapor dome, $dyne/cm^2$

Q_{ann} rate of heat transfer through annular region, cal/sec

Q_{cell} rate of heat transfer through annular region, cal/sec

q heat flux at liquid-vapor interface, cal/(sec)(cm^2)

R_b bottom radius of vapor dome, cm (see fig. 7)

R_{eq} equivalent radius of vapor dome, cm (see fig. 7)

R_0 radius of wire, cm

R_1 radius of liquid-vapor interface, cm

r radial coordinate, cm

T temperature, ^oK

T_f film temperature, ^oK

T_{sat} liquid saturation temperature, ^oK

T_w wire temperature, ^oK

u radial velocity, cm/sec

w axial velocity, cm/sec

x axial coordinate, cm

x_a half length of annular region in cell, cm

β^2 constant of integration given by eq. (B45), cm^2/sec

Γ dimensionless function defined by eq. (F8)

Γ_A asymptotic approximation for Γ_1, eq. (35)

Γ_1 dimensionless function defined by eq. (29), $\Gamma(\Delta = 1)$

Δ ratio of liquid-vapor-interface radius to wire radius, R_1/R_0

δ vapor gap thickness, $R_1 - R_0$, cm

η dimensionless radial coordinate, r/R_0

Λ function defined by eq. (27), cm^{-1}

λ cell wavelength, cm

λ_c critical cell wavelength defined by eq. (1), cm

μ absolute vapor viscosity, g/(cm)(sec)

ν kinematic viscosity of vapor, cm^2/sec

ξ dimensionless axial coordinate, $x/(\lambda/2)$

ξ_a dimensionless annular length, $x_a/(\lambda/2)$

ρ_l liquid density, g/cm^3

ρ_v vapor density, g/cm^3

σ surface tension, dyne/cm

Ψ area correction factor defined by eq. (E8)

ψ stream function, cm^3/sec

Superscript:

(') derivative with respect to independent variable

APPENDIX B

SOLUTION OF FLOW EQUATIONS

Momentum Equations

The momentum equations (eqs. (7) and (8)) can be transformed into one equation with one unknown by introducing the stream function $\psi(r,x)$ in which the continuity equation (eq. (9)) is satisfied identically and the equations of motion (eqs. (7) and (8)) combine to eliminate the pressure terms

$$u = \frac{1}{r}\frac{\partial \psi}{\partial x} \tag{B1}$$

and

$$w = -\frac{1}{r}\frac{\partial \psi}{\partial r} \tag{B2}$$

thereby leading to a single fourth-order equation of the form

$$E^4\psi = 0 \tag{B3}$$

where

$$E^2 = \frac{\partial^2}{\partial r^2} - \frac{1}{r}\frac{\partial}{\partial r} + \frac{\partial^2}{\partial x^2} \tag{B4}$$

If the velocity profiles are assumed to be separable,

$$\psi = f(r)G(x) \tag{B5}$$

equation (B3) takes the form

$$f''''G - \frac{2}{r}f'''G + \frac{3}{r^2}f''G - \frac{3}{r^3}f'G + 2f''G'' - \frac{2}{r}f'G'' + fG'''' = 0 \tag{B6}$$

Now, a set of functions f and g must be chosen which will satisfy the partial differential equation (eq. (B6)) and the boundary conditions. The boundary conditions that apply to the momentum equations (eqs. (11) to (13)), can be expressed in stream function notation as

$$r = R_0 \qquad \frac{\partial \psi}{\partial x} = \frac{\partial \psi}{\partial r} = 0 \tag{B7}$$

$$r = R_1 \qquad \frac{\partial \psi}{\partial x} = \text{Const} \qquad \frac{\partial \psi}{\partial r} = 0 \tag{B8}$$

$$x = 0 \qquad \frac{\partial \psi}{\partial r} = 0 \quad \text{for} \quad R_0 \leq r \leq R_1 \tag{B9}$$

or in terms of f and G

$$r = R_0 \qquad fG' = f'G = 0 \tag{B10}$$

$$r = R_1 \qquad fG' = \text{Const} \qquad f'G = 0 \tag{B11}$$

$$x = 0 \qquad f'G = 0 \quad \text{for} \quad R_0 \leq r \leq R_1 \tag{B12}$$

The functional forms of f and G cannot be obtained directly from equation (B6) because the functions cannot be separated. However, physical intuition and similarity techniques used in references 6 to 8 suggest a functional form in which the radial component of velocity is independent of the axial position

$$G = x \tag{B13}$$

This functional form is consistent with the assumption of a constant vapor gap between the liquid and the wire and the assumed boundary condition that the vaporization velocity $u(R_1)$ is independent of axial position.

Using equation (B13) reduces equation (B6) to the form

$$f'''' - \frac{2}{r} f''' + \frac{3}{r^2} f'' - \frac{3}{r^3} f' = 0 \tag{B14}$$

Multiplying through by r^4 results in

$$r^4 f'''' - 2r^3 f''' + 3r^2 f'' - 3rf' = 0 \tag{B15}$$

which is a fourth-order Cauchy equation (or equidimensional linear equation) having a solution of the form

$$f = a_1 + a_2 r^2 + a_3 r^4 + a_4 r^2 \ln r \tag{B16}$$

Therefore, the stream function defined by equation (B5) takes the form

$$\psi = x(a_1 + a_2 r^2 + a_3 r^4 + a_4 r^2 \ln r) \tag{B17}$$

The analysis was simplified by introducing the following dimensionless variables

$$\xi = \frac{x}{\frac{\lambda}{2}} \tag{B18}$$

$$\eta = \frac{r}{R_0} \tag{B19}$$

Therefore, the stream function becomes

$$\psi = \xi \frac{\lambda}{2} (C_1 + C_2 \eta^2 + C_3 \eta^4 + C_4 \eta^2 \ln \eta) \tag{B20}$$

Velocity Distribution

Substituting equation (B20) into equations (B1) and (B2) results in velocity distributions of the form

$$u = \frac{1}{R_0} \left(\frac{C_1}{\eta} + C_2 \eta + C_3 \eta^3 + C_4 \eta \ln \eta \right) \tag{B21}$$

and

$$w = -\xi \frac{\frac{\lambda}{2}}{R_0^2} \left[2C_2 + 4C_3\eta^2 + C_4(2 \ln \eta + 1)\right] \tag{B22}$$

The boundary conditions given by equations (11) to (13) become

$$\eta = 1 \qquad u = 0 \qquad w = 0 \qquad T = T_w \tag{B23}$$

$$\eta = \Delta \qquad u = u(\Delta) \qquad w = 0 \qquad T = T_{sat} \tag{B24}$$

$$\xi = 0 \qquad w = 0 \quad \text{for} \quad 1 \leq \eta \leq \Delta \tag{B25}$$

where

$$\Delta = \frac{R_1}{R_0} \tag{B26}$$

Applying the boundary conditions, equations (B23) and (B24), to equations (B21) and (B22) results in the following matrix equation:

$$\begin{pmatrix} 1 & 1 & 1 & 0 \\ 0 & 2 & 4 & 1 \\ 0 & 2 & 4\Delta^2 & (2 \ln \Delta + 1) \end{pmatrix} \begin{pmatrix} C_1 \\ C_2 \\ C_3 \\ C_4 \end{pmatrix} = \begin{pmatrix} 0 \\ 0 \\ 0 \end{pmatrix} \tag{B27}$$

Solving this matrix equation by Gauss elimination allows the four constants to be expressed in terms of one constant of integration, called β^2.

$$C_1 = \frac{\beta^2(\ln \Delta + 1 - \Delta^2)}{\ln \Delta} \tag{B28}$$

$$C_2 = \frac{\beta^2(\Delta^2 - 1 - 2 \ln \Delta)}{\ln \Delta} \tag{B29}$$

$$C_3 = \beta^2 \tag{B30}$$

$$C_4 = \frac{2\beta^2(1 - \Delta^2)}{\ln \Delta} \tag{B31}$$

Therefore, the velocity distributions given by equations (B21) and (B22) become

$$u = \frac{\beta^2}{R_0}\left[\frac{\ln \Delta + 1 - \Delta^2}{\eta \ln \Delta} + \frac{(\Delta^2 - 1 - 2 \ln \Delta)\eta}{\ln \Delta} + \eta^3 + 2(1 - \Delta^2)\eta \frac{\ln \eta}{\ln \Delta}\right] \tag{B32}$$

and

$$w = -\frac{\beta^2 \xi \frac{\lambda}{2}}{R_0^2}\left[\frac{2(\Delta^2 - 1 - 2 \ln \Delta)}{\ln \Delta} + 4\eta^2 + \frac{2(2\ln \eta + 1)(1 - \Delta^2)}{\ln \Delta}\right] \tag{B33}$$

The constant β^2 is determined in the section Static Pressure Balance.

Pressure Distribution

The following forms of the momentum equations result from substituting equations (B18) and (B19) into equations (7) and (8):

$$\frac{\partial P}{\partial \eta} = \frac{\mu}{g_c R_0}\left[\frac{\partial^2 u}{\partial \eta^2} + \frac{1}{\eta}\frac{\partial u}{\partial \eta} - \frac{u}{\eta^2} + \left(\frac{R_0}{\frac{\lambda}{2}}\right)^2 \frac{\partial^2 u}{\partial \xi^2}\right] \tag{B34}$$

$$\frac{\partial P}{\partial \xi} = \frac{\mu}{g_c}\frac{\left(\frac{\lambda}{2}\right)}{R_0^2}\left[\frac{\partial^2 w}{\partial \eta^2} + \frac{1}{\eta}\frac{\partial w}{\partial \eta} + \left(\frac{R_0}{\frac{\lambda}{2}}\right)^2 \frac{\partial^2 w}{\partial \xi^2}\right] \tag{B35}$$

Substituting the values of u and w from equations (B32) and (B33) into equations (B34) and (B35) gives

$$\frac{\partial P}{\partial \eta} = \frac{\mu}{g_c R_0} \frac{\beta^2}{R_0} \left[8\eta + \frac{4(1 - \Delta^2)}{\eta \ln \Delta} \right] \tag{B36}$$

$$\frac{\partial P}{\partial \xi} = \frac{-16\mu \left(\frac{\lambda}{2}\right)^2 \beta^2 \xi}{g_c R_0^4} \tag{B37}$$

Integrating equations (B36) and (B37) yields

$$P = \frac{\mu}{g_c} \frac{\beta^2}{R_0^2} \left[4\eta^2 + 4(1 - \Delta^2) \frac{\ln \eta}{\ln \Delta} \right] + F(\xi) + C_5 \tag{B38}$$

$$P = \frac{-8\mu \left(\frac{\lambda}{2}\right)^2 \xi^2 \beta^2}{g_c R_0^4} + H(\eta) + C_5 \tag{B39}$$

Therefore, equating equations (B38) and (B39) results in

$$P = \frac{\mu \beta^2}{g_c R_0^2} \left[4\eta^2 + 4(1 - \Delta^2) \frac{\ln \eta}{\ln \Delta} - 8\xi^2 \left(\frac{\frac{\lambda}{2}}{R_0} \right)^2 \right] + C_5 \tag{B40}$$

The constant C_5 was determined from a simple pressure consideration. The pressure boundary condition given by equation (C3) is

$$P(\Delta, \xi_a) = P_o + \frac{2\sigma}{(1 - \xi_a)\frac{\lambda}{2}} + (1 - \xi_a) \frac{\lambda}{2} \rho_v \frac{a}{g_c} \tag{C3}$$

Evaluating equation (B40) at $\eta = \Delta$ and $\xi = \xi_a$ gives

$$P(\Delta, \xi_a) = \frac{\mu \beta^2}{g_c R_0^2} \left[4 - 8\xi_a^2 \left(\frac{\frac{\lambda}{2}}{R_0} \right)^2 \right] + C_5 \tag{B41}$$

Combining equations (C3) and (B41) and solving for C_5 yield

$$C_5 = P_o + \frac{2\sigma}{(1 - \xi_a)\frac{\lambda}{2}} + (1 - \xi_a)\frac{\lambda}{2}\rho_v \frac{a}{g_c} - \frac{4\mu\beta^2}{g_c R_0^2}\left[1 - 2\xi_a^2\left(\frac{\frac{\lambda}{2}}{R_0}\right)^2\right] \tag{B42}$$

Static Pressure Balance

The theoretical velocity and pressure distributions derived earlier specify these fields with one unknown, β^2. Consequently, an additional mathematical constraint is necessary to determine the velocity and pressure fields.

Substituting equations (B18), (B19), and (B26) into the static pressure balance (eq. (15)) yields

$$\int_0^{\xi_a} P(\Delta, \xi)d\xi = \xi_a \overline{P}_s \tag{B43}$$

Substituting the pressure distribution, equation (B40), into equation (B43) and collecting terms give

$$\beta^2 \frac{4\mu}{g_c R_0^2}\left[1 - \frac{2}{3}\left(\frac{\frac{\lambda}{2}}{R_0}\right)^2 \xi_a^2\right] + C_5 = \overline{P}_s \tag{B44}$$

Substituting the value of C_5 from equation (B42) and equation (C6), which relates P_s and P_o, into equation (B44) give

$$\beta^2 = \frac{(1 - \xi_a)\frac{\lambda}{2}\frac{a}{g_c}(\rho_l - \rho_v) - \frac{2\sigma}{(1 - \xi_a)\frac{\lambda}{2}} + \frac{\sigma}{\Delta R_0}}{\frac{16\mu}{3g_c R_0^2}\left(\frac{\frac{\lambda}{2}}{R_0}\right)^2 \xi_a^2} \tag{B45}$$

The velocity and pressure distribution are now determined explicitly in terms of the cell geometry parameters λ and ξ_a.

Interface Velocity

This analysis predicts a unique relation between the rate of evaporation and the thickness of the vapor gap. This relation arises by substituting $\eta = \Delta$ into equation (B32)

$$u(\Delta) = \frac{\beta^2(\lambda, \xi_a, \Delta)}{R_0 \Delta \ln \Delta}\left[(\ln \Delta)(1 - \Delta^4) + (\Delta^2 - 1)^2\right] \tag{B46}$$

where the constant β^2 is given by equation (B45). Thus, to support the liquid above the wire, an injection velocity $u(\Delta)$ at the liquid-vapor interface is required. Combining equations (B45) and (B46) gives

$$u(\Delta) = \frac{1}{R_0}\left[\frac{(1 - \xi_a)\frac{\lambda}{2}\frac{a}{g_c}(\rho_l - \rho_v) - \frac{2\sigma}{(1 - \xi_a)\frac{\lambda}{2}} + \frac{\sigma}{\Delta R_0}}{\frac{16\mu}{3g_c R_0^2}\left(\frac{\lambda}{2R_0}\right)^2 \xi_a^2}\right]\left[\frac{(\ln \Delta)(1 - \Delta^4) + (\Delta^2 - 1)^2}{\Delta \ln \Delta}\right] \tag{B47}$$

APPENDIX C

ESTIMATE OF PRESSURE AT BASE OF VAPOR DOME

The geometric model shown in figure 2 was redrawn in figure 7. where certain pressures are denoted at key points on the model. The vapor dome was assumed to be spherical as a first approximation. This approximation is fairly accurate for small wires, but not for large wires since the flow tends to be in the vertical direction rather than in the axial direction as assumed in this model. However, the problem resulting from the change in flow direction was overcome by application of equation (16).

If P_o is the pressure in the liquid at the apex of the vapor dome, the pressure at the base of the vapor dome, shown as point P_1 in figure 7, is given by

$$P_1 = P_o + \frac{2\sigma}{(1 - \xi_a)\frac{\lambda}{2}} + (1 - \xi_a)\frac{\lambda}{2}\rho_v \frac{a}{g_c} \tag{C1}$$

Both the pressure jump across a curved interface and the increase in pressure due to a vapor head were considered in equation (C1).

If it is assumed that the pressure drop in the vapor dome is very small (second order),

$$P(\Delta, \xi_a) = P_1 \tag{C2}$$

Therefore,

$$P(\Delta, \xi_a) = P_o + \frac{2\sigma}{(1 - \xi_a)\frac{\lambda}{2}} + (1 - \xi_a)\frac{\lambda}{2}\rho_v \frac{a}{g_c} \tag{C3}$$

This expression is used to determine one constant of integration in the pressure distribution function of appendix B, equation (B40).

Similarly, the pressure in the liquid at the annular liquid-vapor interface is given by

$$P_l = P_o + (1 - \xi_a)\frac{\lambda}{2}\rho_l \frac{a}{g_c} \tag{C4}$$

If the pressure jump across the curved liquid-vapor interface is taken into account, the average pressure $\overline{P}_s$ in the vapor at the annular liquid-vapor interface is defined as

$$\overline{P}_s \equiv P_o + (1 - \xi_a) \frac{\lambda}{2} \rho_l \frac{a}{g_c} + \frac{\sigma}{R_1} \tag{C5}$$

The pressure in the annular vapor region is higher at $\xi = 0$ (centerline of symmetry) than at $\xi = \xi_a$ (base of vapor dome). This pressure difference represents the driving potential for the flow. Therefore, pressure continuity across the interface to some fixed reference requires that, in reality, an annular region of constant radius cannot exist. However, the assumption of a constant annular vapor region (R_1 = constant) makes the problem tractable. Consequently, the pressure $\overline{P}_s$ represents an average vapor pressure between $\xi = 0$ and $\xi = \xi_a$.

Expressing R_1 in terms of Δ and R_0 by equation (B26) yields

$$\overline{P}_s = P_o + (1 - \xi_a) \frac{\lambda}{2} \rho_l \frac{a}{g_c} + \frac{\sigma}{\Delta R_0} \tag{C6}$$

This expression is used in the static pressure balance, equation (B43), to determine the integration constant β^2 (eq. (B45)).

Although the pressure $\overline{P}_s$ and $P(\Delta, \xi_a)$ were obtained at the upper surface of the annular vapor region, the pressure distribution throughout the annular region at any value of ξ may be considered constant as a first-order approximation, thereby limiting the solution to relatively small wires. The average pressure difference between the top and bottom of the annular region is given as

$$\overline{P}_s - \overline{P}_b = 2\rho_v R_1 \frac{a}{g_c} \tag{C7}$$

that is, the pressure difference between the top and bottom interfaces can only differ by the vapor heat existing between the two extremes. Thus, for small wires with large liquid heads

$$\overline{P}_b \cong \overline{P}_s \tag{C8}$$

Clearly, the use of $\overline{P}_s$ in the pressure balance (eq. (B43)) should be accurate at least to a first-order approximation. For large wires, the failure of equation (C8) is of no concern, since the geometric model used in figure 2 breaks down and equation (16) is

introduced to overcome this difficulty.

Some additional interesting facts concerning the shape of the liquid-vapor interface of film boiling on a small wire can be obtained by considering the pressure between the top and bottom liquid-vapor interfaces. In figure 8, the dome region of the geometric model is again shown but in greater detail. For the purposes of the following analysis, the dome is considered to have a shape with an equivalent radius of curvature R_{eq} at the top apex and an equivalent radius of curvature R_b at the bottom apex. The assumption that the top dome is hemispherical is not required here.

The pressure at the point P_{B1} calculated along path 1, which goes through the vapor, equals

$$P_{B1} = P_o + \frac{2\sigma}{R_{eq}} + R_{eq}\rho_v \frac{a}{g_c} + d\rho_v \frac{a}{g_c} \tag{C9}$$

while the pressure at point P_{B2} calculated along path 2, which goes through the liquid equals

$$P_{B2} = P_o + R_{eq}\rho_l \frac{a}{g_c} + d\rho_l \frac{a}{g_c} + \frac{2\sigma}{R_b} \tag{C10}$$

However, from the requirement that the pressure at a given point be independent of the path to that point, the ratio of the radius of curvature at the bottom of the dome R_b to that at the top of the dome can be estimated.

Taking the points B1 and B2 to be at one fixed position, the continuity of pressure requires that

$$P_{B1} = P_{B2} \tag{C11}$$

Substituting equations (C9) and (C10) into equation (C11) yields

$$\frac{R_b}{R_{eq}} = \frac{1}{1 - \dfrac{R_{eq}(R_{eq} + d)(\rho_l - \rho_v)\dfrac{a}{g_c}}{2\sigma}} \tag{C12}$$

Therefore, the radius of curvature beneath the wire R_b is always greater than the radius of curvature at the top of the wire, that is,

$$R_b > R_{eq} \tag{C13}$$

Figure 1(a) shows this in an actual physical situation. This result, of course, applies only to stationary vapor bubbles, since bubbles rising through a liquid are subject to dynamic flow effects.

In addition, the ratio given by equation (C12) must remain positive for physical systems. Thus,

$$\frac{R_{eq}(R_{eq} + d)(\rho_l - \rho_v)\frac{a}{g_c}}{2\sigma} < 1 \tag{C14}$$

Assuming that d is to be small compared with R_{eq} requires that

$$R_{eq} \leq 1.41\left[\frac{\sigma g_c}{(\rho_l - \rho_v)a}\right]^{1/2} \tag{C15}$$

If, the radius of the wire is such that

$$R_0 \geq 1.41\left[\frac{\sigma g_c}{(\rho_l - \rho_v)a}\right]^{1/2} \tag{C16}$$

multiple bubbles might form along the wire since R_{eq} will be less than the diameter of the wire. Thus, the flow would begin to shift from the axial to radial type. Therefore, an estimate for the lower limit of axial flow is given by

$$\frac{l}{D_o} \geq 0.35 \tag{C17}$$

where l is defined by equation (E13).

APPENDIX D

COUPLING OF MOMENTUM AND ENERGY RELATIONS

The momentum and energy relations are coupled by equation (14) which is repeated here in terms of the dimensionless coordinate η:

$$- \rho_v H_{fg} u(\Delta) = - \frac{k}{R_0} \left. \frac{\partial T}{\partial \eta} \right|_{\eta=\Delta} \tag{D1}$$

Substituting the value of the temperature gradient from equation (22) and the value of $u(\Delta)$ from equation (B46) into equation (D1) gives

$$- \frac{\rho_v H_{fg} \beta^2(\lambda, \xi_a, \Delta)}{R_0 \Delta \ln \Delta} \left[(\Delta^2 - 1)^2 + (1 - \Delta^4) \ln \Delta \right] = \frac{k(T_w - T_{sat})}{R_0 \Delta \ln \Delta} \tag{D2}$$

Rearranging equation (D2) yields

$$(\Delta^2 - 1)^2 + (1 - \Delta^4) \ln \Delta = - \frac{k(T_w - T_{sat})}{\rho_v H_{fg} \beta^2(\lambda, \xi_a, \Delta)} \tag{D3}$$

The complete expression for the interface energy balance was obtained by substituting the value of β^2 (eq. (B45)) into equation (D3), which yields

$$(\Delta^2 - 1)^2 + (1 - \Delta^4) \ln \Delta = - \frac{\dfrac{16\, k(T_w - T_{sat}) \mu \left(\dfrac{\lambda}{2R_0} \right)^2 \xi_a^2}{3 \rho_v H_{fg} g_c R_0^2}}{(1 - \xi_a) \dfrac{\lambda}{2} \dfrac{a}{g_c} (\rho_l - \rho_v) - \dfrac{2\sigma}{(1 - \xi_a) \dfrac{\lambda}{2}} + \dfrac{\sigma}{\Delta R_0}} \tag{D4}$$

APPENDIX E

MAXIMIZATION OF ENERGY TRANSPORT

A relation for cell wavelength λ, which until now has remained an unknown parameter, was obtained by using the maximization postulate, equation (17). First, however, an expression for the heat-transfer coefficient was needed.

The total energy transported from the wire to the liquid in a particular cell is given by

$$Q_{ann} = -kA_{ann} \left.\frac{\partial T}{\partial r}\right|_{r=R_0} = -kA_{ann} \frac{1}{R_0} \left.\frac{\partial T}{\partial \eta}\right|_{\eta=1} \tag{E1}$$

where the annular heat-transfer area is given by

$$A_{ann} = A_{cell}\, \Psi(R_0, \xi_a) \tag{E2}$$

with

$$A_{cell} = 2\pi R_0 \lambda \tag{E3}$$

The function $\Psi(R_0, \xi_a)$, represents that fraction of the total area of the cell in which heat is being transferred by conduction. This function can be considered as a correction factor applicable to the large wire problem in which multiple vapor domes appear.

Substituting the expression for the temperature gradient at the wire surfaces (eq. (22)) into equation (E1) results in

$$Q_{ann} = \frac{k(T_w - T_{sat})A_{ann}}{R_0 \ln \Delta} \tag{E4}$$

where Q_{ann} is the local energy transport based on the annular area adjacent to the vapor dome. However, from an experimental point of view the heat-transfer rate and the heat-transfer coefficient are based on the area of the wire. Therefore, the heat transfer in terms of the total cell area is defined by

$$Q_{cell} = h_w(T_w - T_{sat})A_{cell} \tag{E5}$$

but the calculated Q_{ann} heat-transport rates are taken to be equal, that is,

$$Q_{cell} = Q_{ann} \tag{E6}$$

Substituting equations (E4) and (E5) into equation (E6) and rearranging terms yield

$$h_w = \frac{kA_{ann}}{R_0 A_{cell} \ln \Delta} \tag{E7}$$

or, using equation (E2), yield

$$h_w = \frac{k\Psi(R_0, \xi_a)}{R_0 \ln \Delta} \tag{E8}$$

Thus, equation (E8) is an expression for the heat-transfer coefficient for which the maximization hypothesis, equation (17), can be applied.

Substituting equation (E8) into equation (17) and differentiating with respect to λ yield

$$\frac{\partial \Delta}{\partial \lambda} = 0 \tag{E9}$$

Differentiating equation (D3) with respect to λ and using equation (E9) yield

$$\frac{\partial \beta^2}{\partial \lambda} = 0 \tag{E10}$$

Performing the preceding differentiation on β^2 (eq. (B45)) and rearranging terms yield

$$-(1 - \xi_a)\frac{\lambda}{2}(\rho_l - \rho_v)\frac{a}{g_c} + \frac{6\sigma}{(1 - \xi_a)\frac{\lambda}{2}} - \frac{2\sigma}{\Delta R_0}\left(1 + \frac{\lambda}{2\Delta}\frac{d\Delta}{d\lambda}\right) = 0 \tag{E11}$$

According to equation (E9) $d\Delta/d\lambda$ is zero; thus, solving for the cell wavelength yields

$$\frac{\lambda}{2} = \frac{l^2}{(1 - \xi_a)\Delta R_0}\left[\left(1 + \frac{6\Delta^2 R_0^2}{l^2}\right)^{1/2} - 1\right] \tag{E12}$$

$$l = \left[\frac{g_c \sigma}{a(\rho_l - \rho_v)}\right]^{1/2} \tag{E13}$$

Since $\partial^2 h/\partial\lambda^2$ is less than zero, the wavelength defined by equation (E12) is the cell radius that maximizes the heat transfer across the liquid-vapor interface. This optimum arises because heat transfer by conduction directly under the dome is very small. Thus, the dome radius cannot be very large. On the other hand, if λ is very large, a large pressure difference is needed to force the generated vapor into the dome. However, a large pressure difference requires a large dome radius (see appendix C). Thus, it is more efficient, from the point of view of maximizing the heat transport, to have many cells than to have one massive cell (see fig. 1(a)). There is also a limit, however, on the smallness of a cell, since, for infinitely small cells, the surface tension becomes important. If the cell wavelength λ approaches zero, the pressure rise across the vapor dome $2\sigma/R_{eq}$ would become infinite. The pressure in the dome would be greater than that in the surrounding liquid; consequently, the dome could not function as a hydrodynamic sink.

APPENDIX F

HEAT-TRANSFER COEFFICIENT

A simplified expression for the heat-transfer coefficient was derived by using two assumptions (eqs. (23) and (24)). Substituting equation (23) into equation (D3) and rearranging terms give

$$(\Delta - 1) = \left[\frac{3k(T_w - T_{sat})}{4\rho_v H_{fg}\beta^2(\lambda, \xi_a, \Delta)}\right]^{1/4} \tag{F1}$$

This expression represents an interface energy balance between heat conduction and heat loss due to evaporation.

Substituting equation (F1) into equation (25) gives the coefficient for heat transfer from the wire as

$$h_w = \Psi(R_0, \xi_a)\left[\frac{4k^3\rho_v H^*\beta^2}{3(T_w - T_{sat})R_0^4}\right]^{1/4} \tag{F2}$$

where H_{fg} is replaced by H^*, given by equation (3) to take into account sensible effects, as discussed in the introduction.

Some mathematical manipulation is now required to determine the final form of h_w. For convenience, Λ is defined as

$$\Lambda = \frac{1}{\Delta R_0}\left[\left(1 + \frac{6\Delta^2 R_0^2}{l^2}\right)^{1/2} - 1\right] \tag{F3}$$

Thus, substituting equation (F3) into equation (E12) yields

$$\frac{\lambda}{2} = \frac{l^2}{(1 - \xi_a)}\Lambda \tag{F4}$$

In addition, equation (B45) can be written as

$$\beta^2 = \left[\frac{3a(\rho_l - \rho_v)R_0^4}{16\mu l}\right]\left\{\frac{(1 - \xi_a)\frac{\lambda}{2} l}{\left(\frac{\lambda}{2}\right)^2 \xi_a^2}\left[1 - \frac{2l^2}{(1 - \xi_a)^2\left(\frac{\lambda}{2}\right)^2} + \frac{l^2}{\Delta R_0(1 - \xi_a)\frac{\lambda}{2}}\right]\right\} \tag{F5}$$

Substituting equation (F4) into equation (F5) yields

$$\beta^2 = \left[\frac{3a(\rho_l - \rho_v)R_0^4}{16\mu l}\right]\left[\frac{1}{l\Lambda}\left(1 - \frac{2}{l^2\Lambda^2} + \frac{1}{\Delta R_0\Lambda}\right)\right]\left(\frac{1 - \xi_a}{\xi_a}\right)^2 \tag{F6}$$

For mathematical convenience, F(6) is rewritten as

$$\beta^2 = \left[\frac{\sqrt{6}}{48}\left(\frac{1 - \xi_a}{\xi_a}\right)^2\right]\left[\frac{a(\rho_l - \rho_v)R_0^4}{\mu l}\right]\left[\frac{3\sqrt{6}}{2l\Lambda}\left(1 - \frac{2}{l^2\Lambda^2} + \frac{1}{\Delta R_0\Lambda}\right)\right] \tag{F7}$$

Defining

$$\Gamma = \frac{3\sqrt{6}}{2l\Lambda}\left(1 - \frac{2}{l^2\Lambda^2} + \frac{1}{\Delta R_0\Lambda}\right) \tag{F8}$$

gives the expression for β^2 as

$$\beta^2 = \left[\frac{\sqrt{6}}{48}\left(\frac{1 - \xi_a}{\xi_a}\right)^2\right]\left[\frac{a(\rho_l - \rho_v)R_0^4}{\mu l}\right]\Gamma \tag{F9}$$

Substituting this expression for β^2 into the equation for the heat-transfer coefficient (eq. (F2)) yields

$$h_w = \Psi(R_0, \xi_a)\left[\frac{\sqrt{6}}{36}\left(\frac{1 - \xi_a}{\xi_a}\right)^2\right]^{1/4}\left[\frac{k^3 a(\rho_l - \rho_v)H^*\rho_v}{\mu l(T_w - T_{sat})}\right]^{1/4}\Gamma^{1/4} \tag{F10}$$

In applying equation (16), the experimentally verified value of h_∞ of Breen and Westwater (eq. (4)) was used. In terms of l, equation (4) becomes

$$h_\infty = 0.373\left[\frac{k^3 H^* a(\rho_l - \rho_v)\rho_v}{\mu(T_w - T_{sat})l}\right]^{1/4} \tag{F11}$$

Because

$$\lim_{R_0 \to \infty} \Lambda = \frac{\sqrt{6}}{l} \tag{F12}$$

and

$$\lim_{R_0 \to \infty} \Gamma = 1 \tag{F13}$$

it is necessary that

$$\Psi(\infty, \xi_a)\left[\frac{\sqrt{6}}{36}\left(\frac{1 - \xi_a}{\xi_a}\right)^2\right]^{1/4} = 0.373 \tag{F14}$$

Assuming that this condition holds for all values of R_0 gives

$$h_w = 0.373\left[\frac{k^3 H^* a(\rho_l - \rho_v)\rho_v}{\mu(T_w - T_{sat})l}\right]^{1/4} \Gamma^{1/4} \tag{F15}$$

REFERENCES

1. Siegel, Robert; and Keshock, Edward G.: Nucleate and Film Boiling in Reduced Gravity from Horizontal and Vertical Wires. NASA TR R-216, 1965.

2. Lienhard, J. H.; and Wong, P. T. Y.: The Dominant Unstable Wavelength and Minimum Heat Flux During Film Boiling on a Horizontal Cylinder. J. Heat Transfer, vol. 86, no. 2, May 1964, pp. 220-226.

3. Bromley, LeRoy A.: Heat Transfer in Stable Film Boiling. Chem. Engr. Progr., vol. 46, no. 5, May 1950, pp. 221-227.

4. Breen, B. P.; and Westwater, J. W.: Effect of Diameter of Horizontal Tubes on Film Boiling Heat Transfer. Chem. Eng. Progr., vol. 58, no. 7, July 1962, pp. 67-72.

5. Berenson, P. J.: Film-Boiling Heat Transfer from a Horizontal Surface. J. Heat Transfer, vol. 83, no. 3, Aug. 1961, pp. 351-358.

6. Baumeister, K. J.; Hamill, T. D.; Schwartz, F. L.; and Schoessow, G. J.: Film Boiling Heat Transfer to Water Drops on a Flat Plate. AIChE Chem. Engr. Progr. Symp. Ser., vol. 62, no. 64, 1966, pp. 52-61.

7. Baumeister, Kenneth J.; and Hamill, Thomas D.: Creeping Flow Solution of the Leidenfrost Phenomenon. NASA TN D-3133, 1965.

8. Hamill, T. D.; and Baumeister, K. J.: Film Boiling Heat Transfer From a Horizontal Surface as an Optimal Boundary Value Process. Proceedings of the Third International Heat Transfer Conference, Chicago, Aug. 8-12, 1966, ASME, AIChE, 1966, vol. 4, pp. 59-65.

9. Pomerantz, M. L.: Film Boiling on a Horizontal Tube in Increased Gravity Fields. J. Heat Transfer, vol. 86, no. 2, May 1964, pp. 213-219.

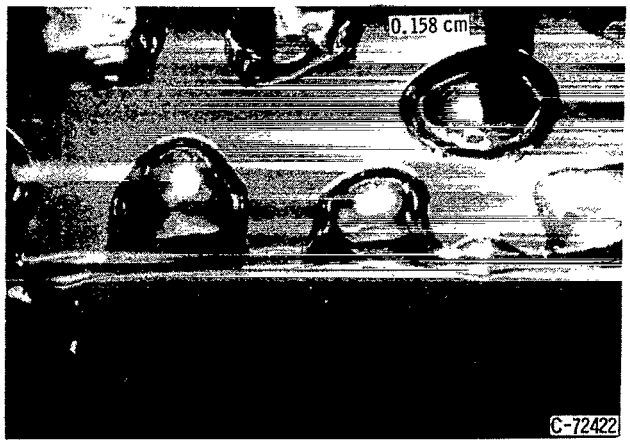

(a) Vapor configuration (ref. 1).

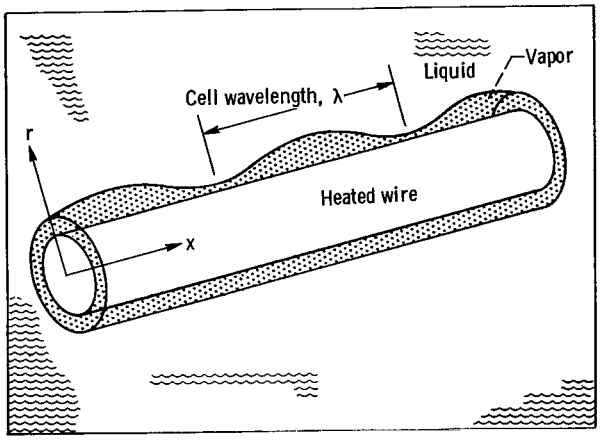

(b) Schematic drawing.

Figure 1. - Film boiling on electrically heated horizontal wire.

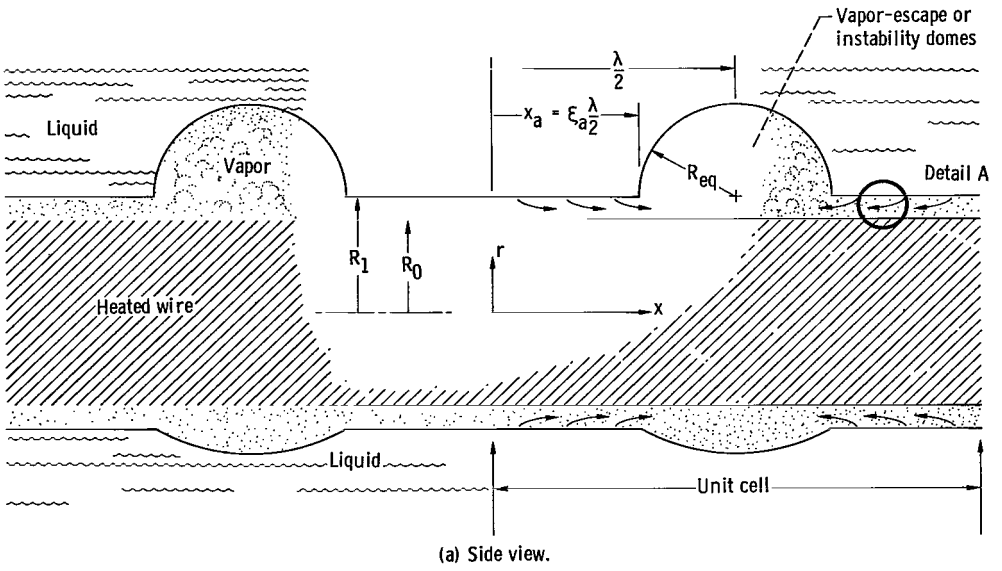

(a) Side view.

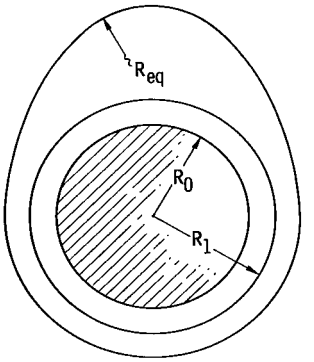

(b) End view.

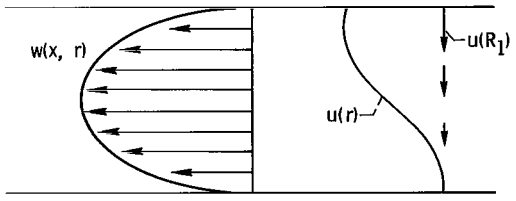

(c) Velocity profiles (detail A).

9002-S

Figure 2. - Geometrical detail of flow model.

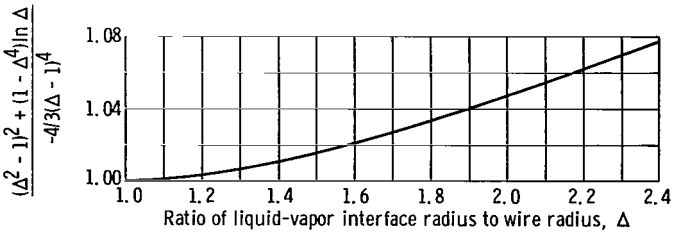

Figure 3. - Ratio of exact to approximate solution of left side of energy balance (eq. (D3)).

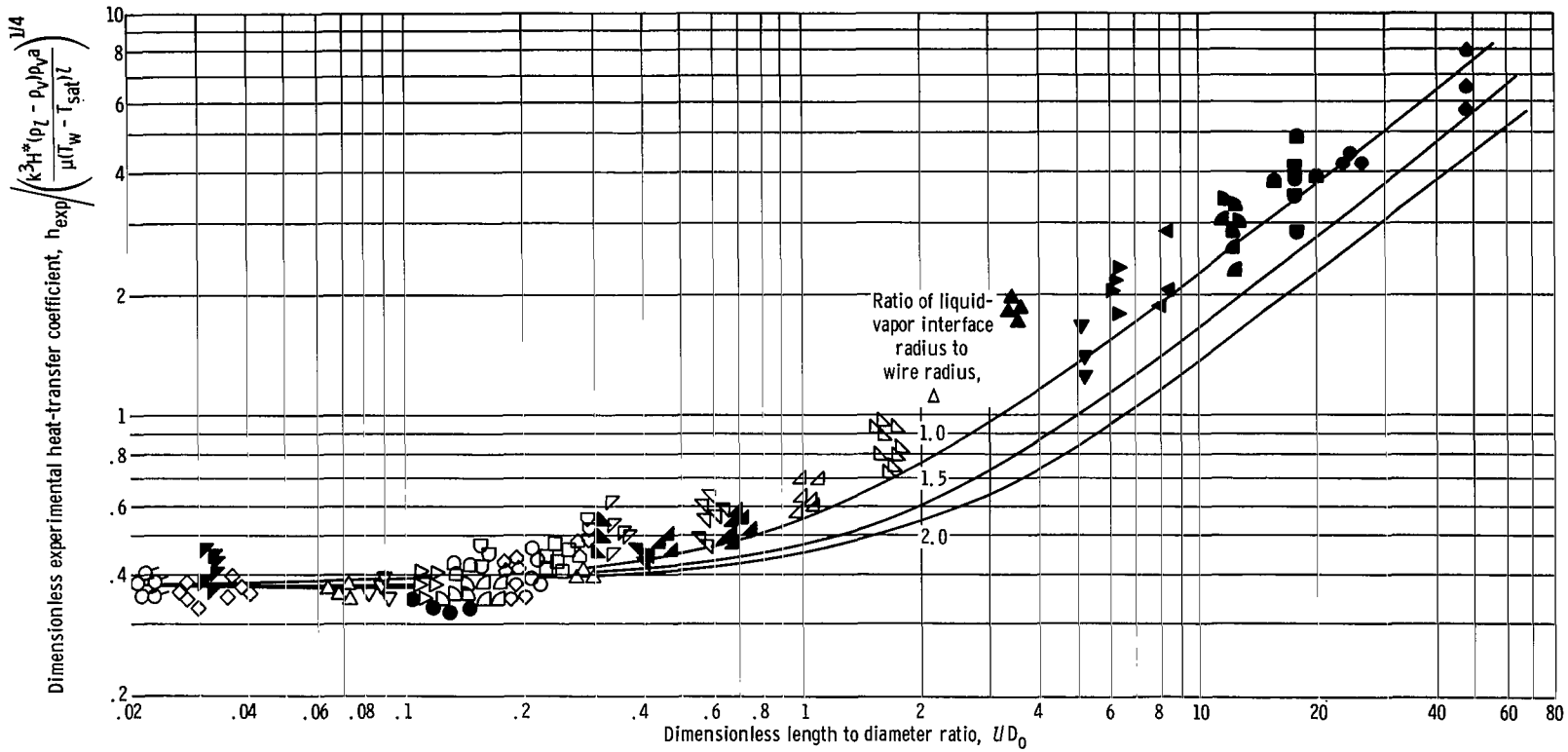

(a) General correlation for various ratios of liquid-vapor interface radius to wire radius.

Figure 4. - Correlations for film boiling on horizontal wires. Wire diameter, 0.00053 to 4.6 centimeters. (Data from ref. 4.) Each type of data point represents a set of test conditions within the following ranges: Fluids, water, helium, oxygen, pentane, nitrogen, ethanol, benzene, Freon 113, isopropanol, or carbon tetrachloride; temperature, 72° to 2600° F; heat-transfer rate 17 to 2120 Btu per hour per square foot per °F; wire diameter, 0.00022 to 1.895 inches; critical wavelength, 0.068 to 0.660 inches; length-diameter ratio, 0.135 to 50.

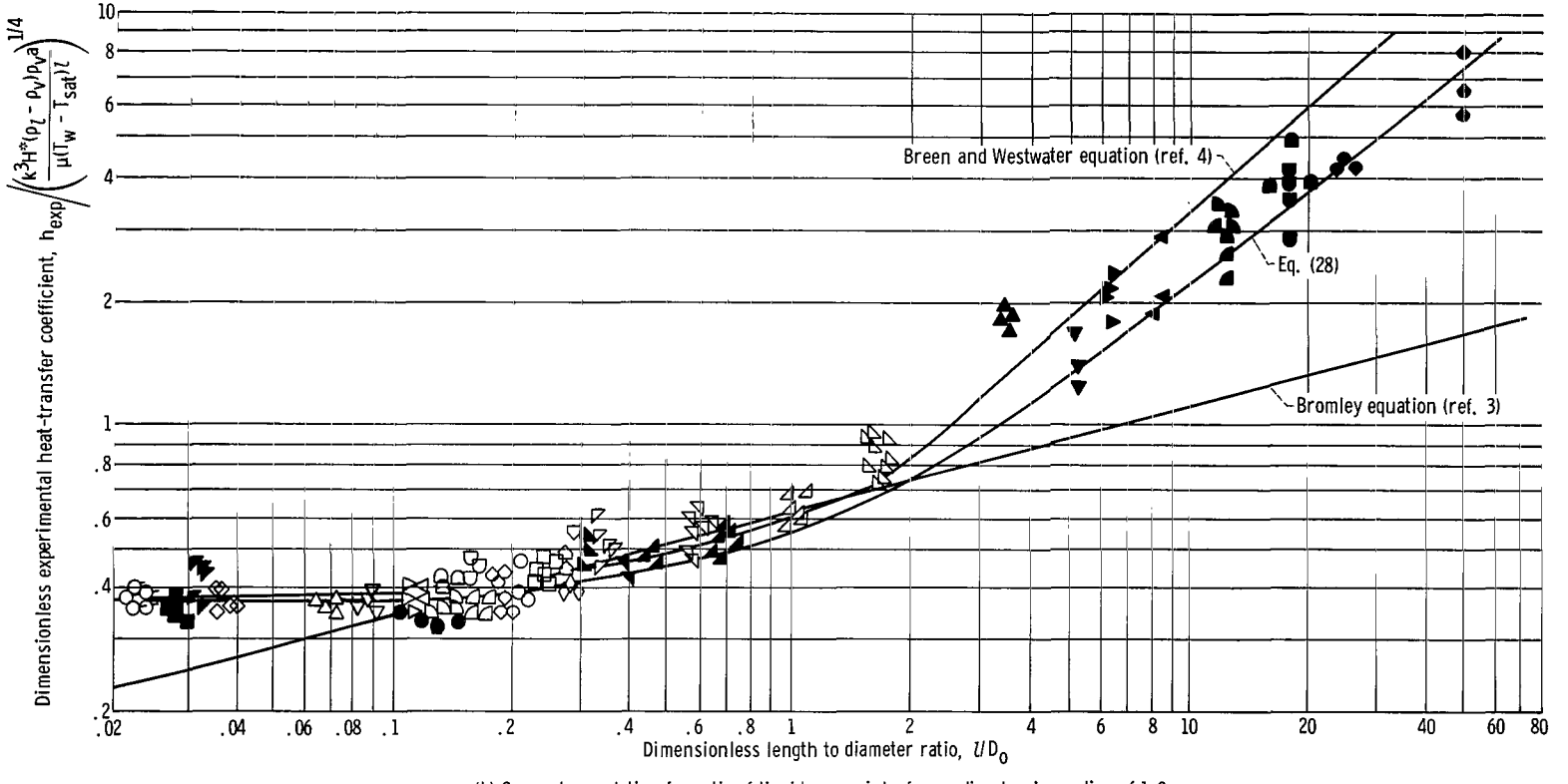

(b) General correlation for ratio of liquid-vapor interface radius to wire radius of 1.0.

Figure 4. - Continued.

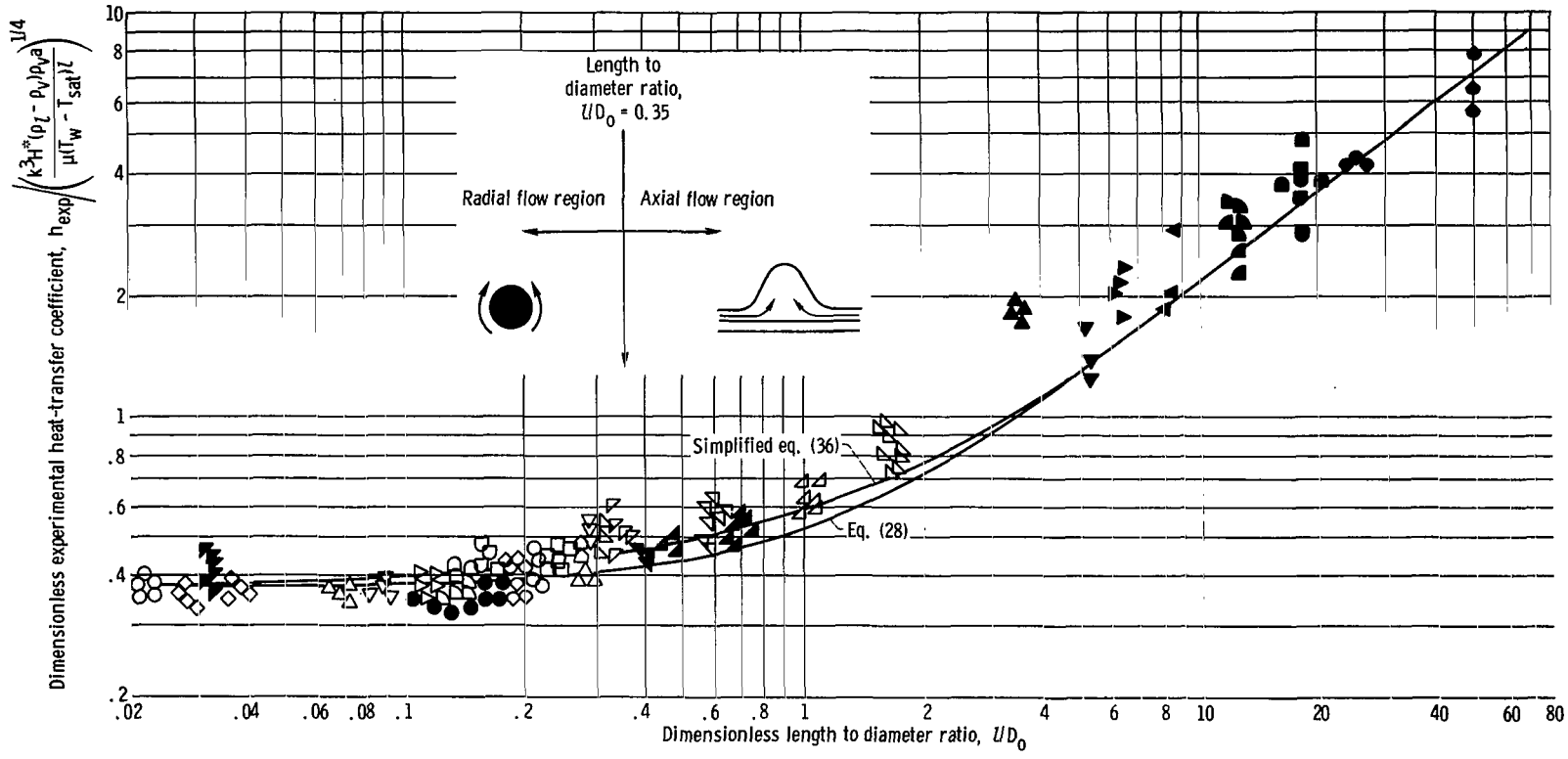

(c) Simplified correlation.

Figure 4. - Concluded.

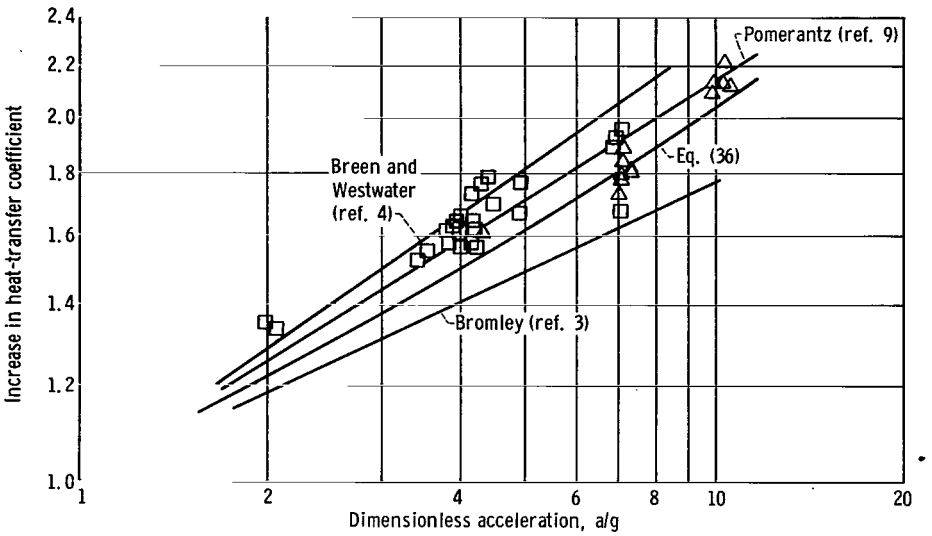

Figure 5. - Influence of acceleration on film boiling in Freon 113 from a horizontal 0.476-centimeter tube (ref. 9).

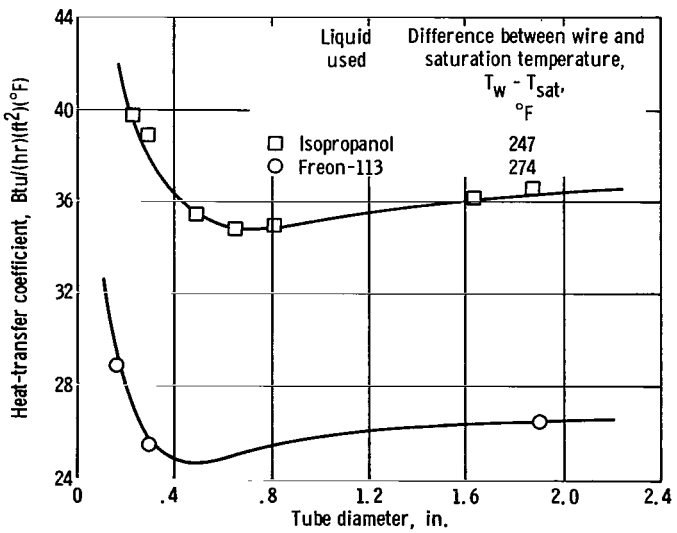

Figure 6. - Heat-transfer coefficients for film boiling from a horizontal tube (ref. 4).

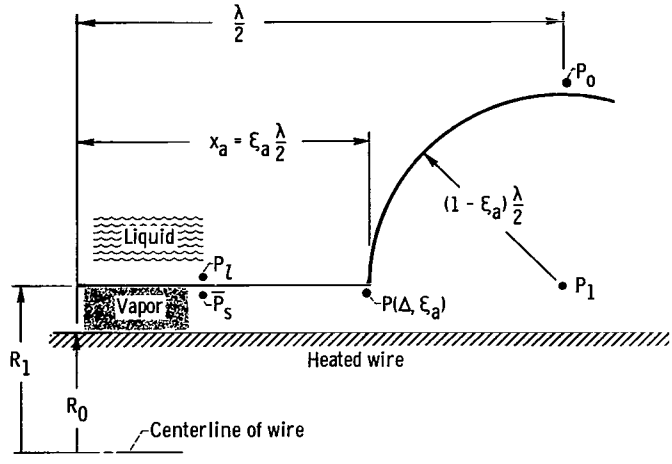

Figure 7. - Pressure points in flow model.

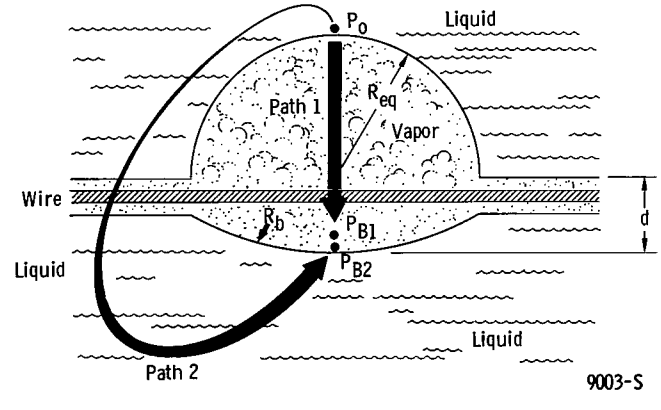

Figure 8. - Calculation paths for determining pressure in vapor dome.

"The aeronautical and space activities of the United States shall be conducted so as to contribute . . . to the expansion of human knowledge of phenomena in the atmosphere and space. The Administration shall provide for the widest practicable and appropriate dissemination of information concerning its activities and the results thereof."

—NATIONAL AERONAUTICS AND SPACE ACT OF 1958

NASA SCIENTIFIC AND TECHNICAL PUBLICATIONS

TECHNICAL REPORTS: Scientific and technical information considered important, complete, and a lasting contribution to existing knowledge.

TECHNICAL NOTES: Information less broad in scope but nevertheless of importance as a contribution to existing knowledge.

TECHNICAL MEMORANDUMS: Information receiving limited distribution because of preliminary data, security classification, or other reasons.

CONTRACTOR REPORTS: Scientific and technical information generated under a NASA contract or grant and considered an important contribution to existing knowledge.

TECHNICAL TRANSLATIONS: Information published in a foreign language considered to merit NASA distribution in English.

SPECIAL PUBLICATIONS: Information derived from or of value to NASA activities. Publications include conference proceedings, monographs, data compilations, handbooks, sourcebooks, and special bibliographies.

TECHNOLOGY UTILIZATION PUBLICATIONS: Information on technology used by NASA that may be of particular interest in commercial and other non-aerospace applications. Publications include Tech Briefs, Technology Utilization Reports and Notes, and Technology Surveys.

Details on the availability of these publications may be obtained from:

SCIENTIFIC AND TECHNICAL INFORMATION DIVISION

NATIONAL AERONAUTICS AND SPACE ADMINISTRATION

Washington, D.C. 20546